Iterative Hybrid Precoding and Combining for Truly Full-Duplex Integrated Sensing and Communication

Murat Bayraktar*, Nuria González-Prelcic*, Roberto López-Valcarce†, Hao Chen‡, and Charlie Jianzhong Zhang‡
*University of California San Diego, USA
†atlanTTic Research Center, Universidade de Vigo, Spain
‡Standards and Mobility Innovation Lab, Samsung Research America, USA
Email:{mbayraktar, ngprelcic}@ucsd.edu, valcarce@gts.uvigo.es, {hao.chen1, jianzhong.z}@samsung.com

***Abstract*—This paper introduces a novel hybrid analog/digital transceiver design for full-duplex (FD) integrated sensing and communication (ISAC) systems operating at mmWave band. The proposed scheme simultaneously supports downlink (DL) and uplink (UL) multiuser communication along with monostatic sensing, while suppressing the self-interference (SI). Considering that high SI levels may lead to saturation at low-noise amplifiers (LNAs), our design incorporates two SI mitigation constraints: one imposed at the receiver (RX) antennas before LNAs and another after the analog combining stage before analog-to-digital converters (ADCs). By formulating optimization problems that balance the trade-offs between spectral efficiency and beampattern error, we leverage a projected gradient ascent (PGA) algorithm with penalty-based methods to iteratively design hybrid precoders and combiners. Simulation results show that the proposed architecture strikes a balance between communication and sensing performance while effectively mitigating SI.**

***Index Terms*—ISAC, full-duplex, self-interference, hybrid precoding and combining, projected gradient ascent.**

I. Introduction

Future wireless communication systems are expected to operate as multifunctional platforms capable of both communication and environmental awareness capabilities. Integrated sensing and communication (ISAC) emerges as a key enabler of this vision, with mmWave frequency bands offering favorable properties for high data rates and high-resolution sensing [1]. Full-duplex (FD) architectures, when applied to ISAC, allow a base station (BS) to concurrently transmit and receive, enabling monostatic sensing in addition to communication [2]. However, this operation introduces self-interference (SI), which can severely degrade receiver (RX) performance.

Existing work on FD ISAC at mmWave has largely focused on downlink (DL) communication-centric designs, where the RX side of the BS is dedicated solely to monostatic sensing [3]–[5]. Although various SI mitigation techniques, such as analog cancellation and SI-aware beamforming, have been proposed, most of these approaches neglect uplink (UL) communication, thus underutilizing the full potential of FD operation. More recent efforts have considered simultaneous DL and UL communication within FD ISAC frameworks using fully digital arrays [6]–[8], assuming idealized scenarios where SI is highly suppressed. Our prior work addressed this problem by introducing a hybrid analog/digital design that supports joint DL/UL communication and sensing in FD ISAC systems [9]. Nonetheless, current hybrid precoding and combining strategies typically suppress SI only after analog combining, i.e., immediately before the analog-to-digital converters (ADCs). This overlooks a critical hardware constraint: high SI levels at the RX antennas can saturate the low-noise amplifiers (LNAs), which are placed before the phase shifters, leading to nonlinear distortion [10]. Additionally, with the exception of [8], most prior works ignore cross-link interference (CLI), which is observed at DL user equipments (UEs) due to concurrent transmission from UL UEs. This is a critical factor in practical FD multiuser systems.

In this paper, we propose a novel hybrid analog/digital transceiver design for wideband mmWave ISAC systems that enables simultaneous DL and UL communication and monostatic sensing. In contrast to prior work, we incorporate constraints on SI not only after the analog combiner but also at the RX antennas, before the LNAs, where high SI levels can cause saturation. These two SI constraints are handled separately: we consider a pre-LNA SI constraint in the hybrid precoder design, and we formulate an analog combiner problem that suppresses the residual SI prior to ADCs. The proposed optimization framework leverages penalty-based methods and projected gradient ascent (PGA) to design the hybrid precoders and combiners. We demonstrate that the proposed design achieves robust communication and sensing performance under realistic SI and CLI conditions.

II. System Model

We consider an FD ISAC system operating at mmWave bands. The transmitter (TX) side of the FD transceiver communicates with U half-duplex DL UEs while the RX side simultaneously receives the data streams transmitted by $\tilde{U}$ half-duplex UL UEs and the echoes reflected by multiple targets. The DL and UL channels are assumed to be perfectly known. The target channels are not known, however, there could be prior information on the target angles. The considered system utilizes OFDM with M subcarriers and N symbols per frame. The TX and RX arrays at the FD ISAC transceiver are equipped with N_{T} and N_{R} antennas, respectively. Both the TX and RX arrays exploit hybrid analog/digital architecture with

This material is based upon work partially supported by the National Science Foundation under grant no. 2433782 and is supported in part by funds from the federal agency and industry partners as specified in the Resilient & Intelligent NextG Systems (RINGS) program and by Samsung Research America.

$N_{\rm RF}$ RF chains. The UEs employ small fully digital arrays with $N_{\rm u}$ antennas. We consider uniform linear arrays (ULAs) with half wavelength spacing for ease of exposition, while the proposed methods can be extended to other architectures.

A. Channel Models

The channel between the FD BS and the u-th DL UE at the m-th subcarrier, $\mathbf{H}_{{\rm dl},u,m} \in \mathbb{C}^{N_{\rm u}\times N_{\rm T}}$, is expressed as

$$\mathbf{H}_{{\rm dl},u,m} = \sum_{l=1}^{L_u} \alpha_l e^{-j2\pi m\tau_l \Delta f} \mathbf{a}_{\rm u}(\phi_l)\mathbf{a}_{\rm T}^{\rm H}(\theta_l), \qquad (1)$$

where L_u is the number of paths. The parameters α_l, τ_l, ϕ_l and θ_l represent the complex channel gain, delay, angle-of-arrival (AoA) and angle-of-departure (AoD) of the l-th path, respectively. The subcarrier spacing is denoted by Δf. The array response vectors at UE arrays are represented by $\mathbf{a}_{\rm u}(\phi) \in \mathbb{C}^{N_{\rm u}}$ for the incident angle ϕ. Similarly, $\mathbf{a}_{\rm T}(\theta) \in \mathbb{C}^{N_{\rm T}}$ denotes the array response at the TX array of the FD BS for the incident angle θ. The channel between the $\tilde{u}$-th UL UE and the FD BS, denoted by $\mathbf{H}_{{\rm ul},\tilde{u},m} \in \mathbb{C}^{N_{\rm R}\times N_{\rm u}}$, follows the same form as (1). Note that this expression includes the array response at the RX array, which is represented by $\mathbf{a}_{\rm R}(\theta) \in \mathbb{C}^{N_{\rm R}}$ for the incident angle θ. Similarly, the CLI channel between the $\tilde{u}$-th UL UE and the u-th DL UE follows the same form as (1), and it is represented by $\mathbf{H}_{{\rm c},u,\tilde{u},m} \in \mathbb{C}^{N_{\rm u}\times N_{\rm u}}$. The described communication channels are assumed to remain constant during a frame. In contrast, we exploit a doubly-selective model for the sensing channel. To that end, we denote the sensing channel that comprises echoes from K point targets by $\mathbf{A}_{m,n} \in \mathbb{C}^{N_{\rm R}\times N_{\rm T}}$ for the m-th subcarrier of the n-th OFDM symbol. Considering that the targets are in the far-field of the FD BS arrays, we assume that the AoA and AoD of a target reflection are the same angle ϑ_k. Thus, the sensing channel is expressed as

$$\mathbf{A}_{m,n} = \sum_{k=0}^{K-1} \xi_k e^{j2\pi(nT_{\rm s}f_{{\rm D},k} - mt_k\Delta f)} \mathbf{a}_{\rm R}(\vartheta_k)\mathbf{a}_{\rm T}^{\rm H}(\vartheta_k), \qquad (2)$$

where $T_{\rm s}$ is the duration of an OFDM symbol. The round-trip time and the Doppler frequency of the target are denoted by t_k and $f_{{\rm D},k}$, respectively. Additionally, complex radar gain of the k-th target is denoted by ξ_k, and is characterized by the radar-range equation $|\xi_k|^2 = \frac{\lambda^2\varsigma_k}{(4\pi)^3 d_k^4}$, where λ is the wavelength, ς_k is the radar cross-section and d_k is the range of the target. Note that the target channel model given in (2) is valid under the following conditions: filtering effects are neglected by assuming the edge subcarriers are left unused so that the frequency response is flat [1]; the largest round-trip time is less than the cyclic prefix duration, and the largest Doppler frequency is much less than the subcarrier spacing.

Finally, we leverage the near-field line-of-sight (LoS) model for the SI channel $\mathbf{H}_{{\rm SI},m} \in \mathbb{C}^{N_{\rm R}\times N_{\rm T}}$, which is expressed as

$$[\mathbf{H}_{{\rm SI},m}]_{p,q} = \frac{\lambda_m}{4\pi d_{pq}} e^{-j2\pi \frac{d_{pq}}{\lambda_m}}, \qquad (3)$$

where λ_m is the wavelength corresponding to m-th subcarrier, and d_{pq} is the distance between the q-th TX antenna and p-th RX antenna [11]. The near-field LoS channel model is a common choice in the literature to characterize the strong SI channel since there are no established models. It is also possible to include non-LoS (NLoS) reflections in this channel, which would not affect the proposed methods in this paper since they are agnostic to the SI channel model.

B. Received Signals

We first introduce the precoders and combiners employed at the FD BS and UEs before describing the received signals. Since the FD BS employs a hybrid analog/digital architecture, the frequency-flat and UE independent analog precoder with unit-modulus entries is defined as $\mathbf{F}_{\rm RF} \in \mathbb{C}^{N_{\rm T}\times N_{\rm RF}}$, while the digital precoder for the u-th DL UE at m-th subcarrier is represented by $\mathbf{f}_{{\rm BB},u,m} \in \mathbb{C}^{N_{\rm RF}}$. Additionally, overall digital combiners can be constructed as $\mathbf{F}_{{\rm BB},m} = [\mathbf{f}_{{\rm BB},1,m}, \ldots, \mathbf{f}_{{\rm BB},U,m}]$. Moreover, the digital combiner applied at the u-th DL UE is denoted by $\mathbf{u}_{u,m} \in \mathbb{C}^{N_{\rm u}}$. The data symbol transmitted to the u-th DL UE at m-th subcarrier of the n-th OFDM symbol is represented by $d_{u,m,n}$, and the overall data vector can be constructed as $\mathbf{d}_{m,n} = [d_{1,m,n}, \ldots, d_{U,m,n}]^{\rm T}$. Note that the data symbols have unit power and they are independent for each UE. With these descriptions, the received signal after the combiner of u-th DL UE is expressed as

$$\begin{aligned} r_{u,m,n} &= \mathbf{u}_{u,m}^{\rm H}\mathbf{H}_{{\rm dl},u,m}\mathbf{F}_{\rm RF}\mathbf{f}_{{\rm BB},u,m}d_{u,m,n} \\ &\quad + \mathbf{u}_{u,m}^{\rm H}\sum_{i\neq u}^{U-1}\mathbf{H}_{{\rm dl},u,m}\mathbf{F}_{\rm RF}\mathbf{f}_{{\rm BB},i,m}d_{i,m,n} \\ &\quad + \mathbf{u}_{u,m}^{\rm H}\sum_{\tilde{u}=0}^{\tilde{U}-1}\mathbf{H}_{{\rm c},u,\tilde{u},m}\mathbf{v}_{\tilde{u},m}s_{\tilde{u},m,n} + \mathbf{u}_{u,m}^{\rm H}\mathbf{z}_{u,m,n}, \qquad (4) \end{aligned}$$

where $\mathbf{z}_{u,m,n} \in \mathbb{C}^{N_{\rm u}}$ is the noise vector with covariance $\mathbb{E}\left\{\mathbf{z}_{u,m,n}\mathbf{z}_{u,m,n}^{\rm H}\right\} = \sigma_u^2\mathbf{I}_{N_{\rm u}}$. Furthermore, the digital precoder and the data symbol of the $\tilde{u}$-th UL UE with unit power at the m-th subcarrier of the n-th OFDM symbol are given by $\mathbf{v}_{\tilde{u},m} \in \mathbb{C}^{N_{\rm u}}$ and $s_{\tilde{u},m,n}$, respectively. The first term in (4) is the intended signal for the u-th DL UE, while the second term represents the multiuser interference. The following term is the CLI caused by the simultaneous transmission at the UL UEs. Finally, the last term is the noise after the combiner.

Considering that the analog combiner $\mathbf{W}_{\rm RF} \in \mathbb{C}^{N_{\rm R}\times N_{\rm RF}}$ is used at the FD BS, the received signal $\mathbf{y}_{m,n} \in \mathbb{C}^{N_{\rm RF}}$ at the output of the RF chains can be expressed as

$$\begin{aligned} \mathbf{y}_{m,n} &= \mathbf{W}_{\rm RF}^{\rm H}\sum_{\tilde{u}=0}^{\tilde{U}-1}\mathbf{H}_{{\rm ul},\tilde{u},m}\mathbf{v}_{\tilde{u},m}s_{\tilde{u},m,n} \\ &\quad + \mathbf{W}_{\rm RF}^{\rm H}(\mathbf{H}_{{\rm SI},m}+\mathbf{A}_{m,n})\mathbf{F}_{\rm RF}\mathbf{F}_{{\rm BB},m}\mathbf{d}_{m,n}+\mathbf{W}_{\rm RF}^{\rm H}\mathbf{n}_{m,n}, \qquad (5) \end{aligned}$$

where $\mathbf{n}_{m,n} \in \mathbb{C}^{N_{\rm R}}$ is the noise vector with covariance $\mathbb{E}\left\{\mathbf{n}_{m,n}\mathbf{n}_{m,n}^{\rm H}\right\} = \tilde{\sigma}^2\mathbf{I}_{N_{\rm R}}$. The first term comprises the UL signals, while the second term includes the SI and target reflections. The last term is the noise after the analog combiner. The analog combiner should support both communication and sensing directions since it is frequency-flat and UE independent. It is important to note that UL signals create interference to each other and also to the targets signals, and vice versa. Thus, they should be separated via the digital combiners. The digital combiner of the $\tilde{u}$-th UL UE is denoted by $\mathbf{v}_{\tilde{u},m}\mathbb{C}^{N_{\mathrm{RF}}}$, and the received signal after this combiner can be written as

$$\begin{aligned} y_{\tilde{u},m,n} &= \mathbf{w}_{\mathrm{BB},\tilde{u},m}^{\mathrm{H}}\mathbf{W}_{\mathrm{RF}}^{\mathrm{H}}\mathbf{H}_{\mathrm{ul},\tilde{u},m}\mathbf{v}_{\tilde{u},m}s_{\tilde{u},m,n} \\ &+ \mathbf{w}_{\mathrm{BB},\tilde{u},m}^{\mathrm{H}}\mathbf{W}_{\mathrm{RF}}^{\mathrm{H}}\sum_{j\neq\tilde{u}}^{\tilde{U}-1}\mathbf{H}_{\mathrm{ul},j,m}\mathbf{v}_{j,m}s_{j,m,n} \\ &+ \mathbf{w}_{\mathrm{BB},\tilde{u},m}^{\mathrm{H}}\mathbf{W}_{\mathrm{RF}}^{\mathrm{H}}(\mathbf{H}_{\mathrm{SI},m}+\mathbf{A}_{m,n})\mathbf{F}_{\mathrm{RF}}\mathbf{F}_{\mathrm{BB},m}\mathbf{d}_{m,n} \\ &+ \mathbf{w}_{\mathrm{BB},\tilde{u},m}^{\mathrm{H}}\mathbf{W}_{\mathrm{RF}}^{\mathrm{H}}\mathbf{n}_{m,n}, \end{aligned} \tag{6}$$

where the intended signal for $\tilde{u}$-th UL UE and the multiuser interference are separated as the first two terms. While it is not explicitly discussed in this work, it is assumed that the radar processing algorithms are applied after the analog combiner. It is possible to suppress the interference caused by UL UEs and residual SI via interference-aware digital filters and OFDM radar [9]. However, this stage is out of the scope of this paper.

III. Problem Formulation

The design goal of the FD ISAC system is to enable simultaneous communication and sensing while suppressing the SI. This problem is usually intractable, especially with the hybrid analog/digital architectures [1]. Thus, we simplify it and focus on the hybrid precoding and combining design at the FD BS. To that end, we assume that the UEs have information only about their own channels, which are used to design their respective precoders and combiners. Note that this is a practical choice that reduces the feedback overhead.

While other choices are possible, we assume that the precoders/combiners at the UL/DL UEs are designed with the optimal SVD-based approach that ideally maximizes the communication rate in a half-duplex single-user communication system. That is, the combiner of the u-th DL UE at the m-th subcarrier (i.e., $\mathbf{u}_{u,m}$) is selected as the left singular vector that corresponds to the largest singular value of the channel matrix $\mathbf{H}_{\mathrm{dl},u,m}$. Analogously, the precoder of the $\tilde{u}$-th UL UE at the m-th subcarrier (i.e., $\mathbf{v}_{\tilde{u},m}$) is designed with the right singular vector corresponding to the largest singular value of the channel matrix $\mathbf{H}_{\mathrm{ul},\tilde{u},m}$. We assume that the singular vectors used as the precoders at UL UEs are scaled with their transmit power $\tilde{P}_{\mathrm{t},\tilde{u}}$. Given the precoders and combiners, the effective DL, UL and CLI channels are expressed as $\bar{\mathbf{h}}_{\mathrm{dl},u,m} = \mathbf{H}_{\mathrm{dl},u,m}^{\mathrm{H}}\mathbf{u}_{u,m}$, $\bar{\mathbf{h}}_{\mathrm{ul},\tilde{u},m} = \mathbf{H}_{\mathrm{ul},\tilde{u},m}\mathbf{v}_{\tilde{u},m}$ and $h_{\mathrm{c},u,\tilde{u},m} = \mathbf{u}_{u,m}^{\mathrm{H}}\mathbf{H}_{\mathrm{c},u,\tilde{u},m}\mathbf{v}_{\tilde{u},m}$, respectively. It is assumed that the FD BS acquires the effective DL and UL channels either via feedback or estimation. Furthermore, the DL UEs do not explicitly estimate the effective CLI channels, however, it is reasonable to assume that they estimate the effective interference-plus-noise level that can be written as $\bar{\sigma}_u^2 = \sum_{\tilde{u}}|h_{\mathrm{c},u,\tilde{u},m}|^2 + \sigma_u^2$.

In the following, we formulate the hybrid precoder and combiner design problems. As a final simplification, we utilize sequential optimization such that the precoder is designed first, and then the combiner is designed with the given precoder.

A. Hybrid Precoder Design at FD BS

We first define the metrics to be optimized for the hybrid precoder design. We use spectral efficiency achieved at DL UEs as the communication metric. Specifically, the spectral efficiency of u-th DL UE at m-th subcarrier is expressed as

$$\mathcal{R}_{u,m} = \log_2\left(1+\frac{\left|\bar{\mathbf{h}}_{\mathrm{dl},u,m}^{\mathrm{H}}\mathbf{F}_{\mathrm{RF}}\mathbf{f}_{\mathrm{BB},u,m}\right|^2}{\sum_{i\neq u}\left|\bar{\mathbf{h}}_{\mathrm{dl},u,m}^{\mathrm{H}}\mathbf{F}_{\mathrm{RF}}\mathbf{f}_{\mathrm{BB},i,m}\right|^2+\bar{\sigma}_u^2}\right). \tag{7}$$

The sensing metric depends on the considered scenario. For example, the goal could be detecting targets in an angular region, or tracking the targets located at pre-estimated angles. Without loss of generality, we consider a tracking scenario where the estimates of the target angles are available. We utilize the radar beampattern error as the sensing metric, which essentially aims to optimize the covariance of the hybrid precoders for a given target angle ϑ_k as

$$\mathcal{B}_m(\vartheta_k) = \left|\mathcal{P}(\vartheta_k) - \mathbf{a}_{\mathrm{T}}^{\mathrm{H}}(\vartheta_k)\mathbf{F}_{\mathrm{RF}}\mathbf{F}_{\mathrm{BB},m}\mathbf{F}_{\mathrm{BB},m}^{\mathrm{H}}\mathbf{F}_{\mathrm{RF}}^{\mathrm{H}}\mathbf{a}_{\mathrm{T}}(\vartheta_k)\right|^2, \tag{8}$$

where $\mathcal{P}(\vartheta_k)$ is the desired beam gain at target angle ϑ_k. The precoder design goal is to minimize the average beampattern error for a set of angles, which has been widely adopted in the literature [12]–[14]. Another metric that the precoder design needs consider is the SI observed at each RX antenna, i.e., before the signal reaches the LNAs. The SI power observed at the p-th RX antenna and m-th subcarrier is expressed as

$$\mathcal{S}_{p,m} = \left\|\left[\mathbf{H}_{\mathrm{SI},m}\mathbf{F}_{\mathrm{RF}}\mathbf{F}_{\mathrm{BB},m}\right]_{p,:}\right\|^2. \tag{9}$$

Additionally, the residual SI observed at the output of the analog combiner, i.e., before the ADCs, should be limited. However, this would require the joint optimization of the hybrid precoders and analog combiner, which would add to the complexity of the problem. Thus, we only consider the SI at RX antennas while designing the precoder, and the SI observed after the analog combiner is considered in the combiner design problem. We consider a weighted objective function that comprises the sum DL spectral efficiency and the average beampattern error. Note that the objective function is averaged over all subcarriers. Furthermore, the SI power at RX antennas are constrained to be below a threshold γ. This problem can be expressed as

$$\begin{aligned} \underset{\mathbf{F}_{\mathrm{RF}},\mathbf{F}_{\mathrm{BB},m}}{\text{maximize}} \quad & \frac{1}{M}\sum_{m=0}^{M-1}(\mathcal{R}_m - \mu_{\mathrm{b}}\mathcal{B}_m) \\ \text{subject to} \quad & \mathcal{S}_{p,m}\leq\gamma,\ \forall p,m, \\ & |[\mathbf{F}_{\mathrm{RF}}]_{p,q}| = 1,\ \forall p,q, \\ & \|\mathbf{F}_{\mathrm{RF}}\mathbf{F}_{\mathrm{BB},m}\|_{\mathrm{F}}^2 = P_{\mathrm{t}}, \forall m, \end{aligned} \tag{10}$$

where the sum DL spectral efficiency and average beampattern error are defined as $\mathcal{R}_m = \sum_{u=0}^{U-1}\mathcal{R}_{u,m}$ and $\mathcal{B}_m = \frac{1}{K}\sum_{k=0}^{K-1}\mathcal{B}_m(\vartheta_k)$, respectively. The weight μ_{b} determines the emphasis put on minimizing $\mathcal{B}_m$. Furthermore, the constraint before the last one is the unit modulus constraint on the analog precoder entries, and the last one is the power constraint at each subcarrier with P_{t} being the transmit power.

B. Hybrid Combiner Design at FD BS

Analogous to the precoder design problem, we consider the spectral efficiency of each UL UE as the communication metric. The spectral efficiency expression for the $\tilde{u}$-th UL UE

$$\tilde{\mathcal{R}}_{\tilde{u},m} = \log_2\left(1 + \frac{\tilde{P}_{\mathrm{t},\tilde{u}}\left|\mathbf{w}_{\mathrm{BB},\tilde{u},m}^{\mathrm{H}}\mathbf{W}_{\mathrm{RF}}^{\mathrm{H}}\bar{\mathbf{h}}_{\mathrm{ul},\tilde{u},m}\right|^2}{\sum_{j\neq\tilde{u}}\tilde{P}_{\mathrm{t},j}\left|\mathbf{w}_{\mathrm{BB},\tilde{u},m}^{\mathrm{H}}\mathbf{W}_{\mathrm{RF}}^{\mathrm{H}}\bar{\mathbf{h}}_{\mathrm{ul},j,m}\right|^2 + \left\|\mathbf{w}_{\mathrm{BB},\tilde{u},m}^{\mathrm{H}}\mathbf{W}_{\mathrm{RF}}^{\mathrm{H}}(\mathbf{H}_{\mathrm{SI},m}+\mathbf{A}_{m,n})\mathbf{F}_{\mathrm{RF}}\mathbf{F}_{\mathrm{BB},m}\right\|^2 + \tilde{\sigma}^2\left\|\mathbf{W}_{\mathrm{RF}}\mathbf{w}_{\mathrm{BB},\tilde{u},m}\right\|^2}\right) \tag{11}$$

at m-th subcarrier is given in (11) on the top of this page. For the sensing metric, we consider the beampattern error at the output of the analog combiner, which is expressed as

$$\tilde{\mathcal{B}}(\vartheta_k) = \left|\mathcal{P}(\vartheta_k) - \mathbf{a}_{\mathrm{R}}^{\mathrm{H}}(\vartheta_k)\mathbf{W}_{\mathrm{RF}}\mathbf{W}_{\mathrm{RF}}^{\mathrm{H}}\mathbf{a}_{\mathrm{R}}(\vartheta_k)\right|^2, \tag{12}$$

for target angle ϑ_k. This term does not depend on the subcarrier index m. Finally, the residual SI observed at the output of the q-th RX RF chain and m-th subcarrier is expressed as

$$\tilde{\mathcal{S}}_{q,m} = \left\|\left[\mathbf{W}_{\mathrm{RF}}^{\mathrm{H}}\mathbf{H}_{\mathrm{SI},m}\mathbf{F}_{\mathrm{RF}}\mathbf{F}_{\mathrm{BB},m}\right]_{q,:}\right\|^2. \tag{13}$$

Following the same approach as done in the hybrid precoder design, we utilize a weighted sum as the objective function. Moreover, the residual SI at the output of each RF chain is bounded by a threshold $\tilde{\gamma}$. This problem can be expressed as

$$\begin{aligned} \underset{\mathbf{W}_{\mathrm{RF}},\mathbf{W}_{\mathrm{BB},m}}{\text{maximize}} \quad & \frac{1}{M}\sum_{m=0}^{M-1}\tilde{\mathcal{R}}_m - \tilde{\mu}_{\mathrm{b}}\tilde{\mathcal{B}} \\ \text{subject to} \quad & \tilde{\mathcal{S}}_{q,m} \le \tilde{\gamma}, \forall q, \\ & |[\mathbf{W}_{\mathrm{RF}}]_{p,q}| = 1,\ \forall p,q, \end{aligned} \tag{14}$$

where $\tilde{\mathcal{R}}_m = \sum_{\tilde{u}=0}^{\tilde{U}-1}\tilde{\mathcal{R}}_{\tilde{u},m}$ and $\tilde{\mathcal{B}} = \frac{1}{K}\sum_{k=0}^{K-1}\tilde{\mathcal{B}}(\vartheta_k)$. The weight $\tilde{\mu}_{\mathrm{b}}$ is adjusts the communication and sensing trade-off.

IV. Projected Gradient Ascent Solution

In this section, we introduce a PGA-based solution that is applicable to both hybrid precoder and combiner design. First, we note that the problems in (10) and (14) are non-convex due to the unit-modulus constraint imposed on the analog precoder and combiner. Additionally, there is a strong coupling between the digital and analog parts in both optimization problems. Thus, we optimize them in an alternating fashion.

A. Precoder Optimization

For iterative projection-based algorithms, such as PGA, the problem in (10) can be solved by neglecting the unit-modulus and power constraints that can be enforced via projection after each iteration [15]. The SI constraint prevents us from using the PGA algorithm since gradient-based optimizers are aimed to solve unconstrained problems. We initially neglect the threshold γ and move the SI constraint to the objective function as a penalty term as done in [6]. However, we will monitor if the maximum SI observed at RX antennas satisfies the threshold constraint during PGA iterations, and adjust the value of the penalty weight according to constraint violations, which is a common approach in penalty-based methods [16]. Thus, reformulated problem can be expressed as

$$\begin{aligned} \underset{\mathbf{F}_{\mathrm{RF}},\mathbf{F}_{\mathrm{BB},m}}{\text{maximize}} \quad & \frac{1}{M}\sum_{m=0}^{M-1}\left(\mathcal{R}_m - \mu_{\mathrm{b}}\mathcal{B}_m(\vartheta_k) - \mu_{\mathrm{SI}}\mathcal{S}_m\right) \\ \text{subject to} \quad & |[\mathbf{F}_{\mathrm{RF}}]_{p,q}| = 1,\ \forall p,q, \\ & \|\mathbf{F}_{\mathrm{RF}}\mathbf{F}_{\mathrm{BB},m}\|_{\mathrm{F}}^2 = P_{\mathrm{t}}, \forall m, \end{aligned} \tag{15}$$

where $\mathcal{S}_m = \sum_{p=1}^{N_{\mathrm{R}}}\mathcal{S}_{p,m} = \|\mathbf{H}_{\mathrm{SI},m}\mathbf{F}_{\mathrm{RF}}\mathbf{F}_{\mathrm{BB},m}\|_{\mathrm{F}}^2$, and μ_{SI} is the common penalty weight for the SI observed at all RX antennas. While separate penalty weights could be used for RX antennas, we consider a common penalty term for simplicity. In PGA, we omit the constraints in (15), and update the variables by using the gradient of the objective function. Then, we project the updated variable to the feasible set. The gradient of the objective function in (15), denoted by $\mathcal{C}$, with respect to $\mathbf{F}_{\mathrm{RF}}$ is expressed as

$$\begin{aligned} \nabla_{\mathbf{F}_{\mathrm{RF}}}\mathcal{C} = \frac{1}{M}\sum_{m=0}^{M-1}\Bigg(&\sum_{u=1}^{U}\nabla_{\mathbf{F}_{\mathrm{RF}}}\mathcal{R}_{u,m} \\ &- \mu_{\mathrm{b}}\nabla_{\mathbf{F}_{\mathrm{RF}}}\frac{1}{K}\sum_{k=0}^{K-1}\mathcal{B}_m(\vartheta_k) - \mu_{\mathrm{SI}}\nabla_{\mathbf{F}_{\mathrm{RF}}}\mathcal{S}_m\Bigg). \end{aligned} \tag{16}$$

We omit the derivations of the gradients and give the final expressions due to space limitation. The gradients $\nabla_{\mathbf{F}_{\mathrm{RF}}}\mathcal{R}_{u,m}$, $\nabla_{\mathbf{F}_{\mathrm{RF}}}\mathcal{B}_m(\vartheta_k)$ and $\nabla_{\mathbf{F}_{\mathrm{RF}}}\mathcal{S}_m$ are expressed as follows

$$\begin{aligned} \nabla_{\mathbf{F}_{\mathrm{RF}}}\mathcal{R}_{u,m} = &\frac{\bar{\mathbf{h}}_{\mathrm{dl},u,m}\bar{\mathbf{h}}_{\mathrm{dl},u,m}^{\mathrm{H}}\mathbf{F}_{\mathrm{RF}}\mathbf{F}_{\mathrm{BB},m}\mathbf{F}_{\mathrm{BB},m}^{\mathrm{H}}}{\ln 2\cdot\left(\left\|\bar{\mathbf{h}}_{\mathrm{dl},u,m}^{\mathrm{H}}\mathbf{F}_{\mathrm{RF}}\mathbf{F}_{\mathrm{BB},m}\right\|^2 + \bar{\sigma}_u^2\right)} \\ &- \frac{\bar{\mathbf{h}}_{\mathrm{dl},u,m}\bar{\mathbf{h}}_{\mathrm{dl},u,m}^{\mathrm{H}}\mathbf{F}_{\mathrm{RF}}\mathbf{F}_{\mathrm{BB},m}\mathbf{E}_u\mathbf{F}_{\mathrm{BB},m}^{\mathrm{H}}}{\ln 2\cdot\left(\left\|\bar{\mathbf{h}}_{\mathrm{dl},u,m}^{\mathrm{H}}\mathbf{F}_{\mathrm{RF}}\mathbf{F}_{\mathrm{BB},m}\mathbf{E}_u\right\|^2 + \bar{\sigma}_u^2\right)}, \end{aligned} \tag{17}$$

$$\nabla_{\mathbf{F}_{\mathrm{RF}}}\mathcal{B}_m(\vartheta_k) = -2\sqrt{\mathcal{B}_m(\vartheta_k)}\mathbf{A}_{\mathrm{T}}(\vartheta_k)\mathbf{F}_{\mathrm{RF}}\mathbf{F}_{\mathrm{BB},m}\mathbf{F}_{\mathrm{BB},m}^{\mathrm{H}}, \tag{18}$$

$$\nabla_{\mathbf{F}_{\mathrm{RF}}}\mathcal{S}_m = \mathbf{H}_{\mathrm{SI},m}\mathbf{H}_{\mathrm{SI},m}^{\mathrm{H}}\mathbf{F}_{\mathrm{RF}}\mathbf{F}_{\mathrm{BB},m}\mathbf{F}_{\mathrm{BB},m}^{\mathrm{H}}, \tag{19}$$

where $\mathbf{A}_{\mathrm{T}}(\vartheta_k) = \mathbf{a}_{\mathrm{T}}(\vartheta_k)\mathbf{a}_{\mathrm{T}}^{\mathrm{H}}(\vartheta_k)$, and $\mathbf{E}_u$ is a diagonal matrix with $[\mathbf{E}_u]_{i,i} = 1$ for $i \neq u$. Similarly, the gradient of the objective function $\mathcal{C}$ with respect to $\mathbf{F}_{\mathrm{BB},m}$ is expressed as

$$\begin{aligned} \nabla_{\mathbf{F}_{\mathrm{BB},m}}\mathcal{C} = \frac{1}{M}\sum_{m=0}^{M-1}\Bigg(&\sum_{u=1}^{U}\nabla_{\mathbf{F}_{\mathrm{BB},m}}\mathcal{R}_{u,m} \\ &- \mu_{\mathrm{b}}\nabla_{\mathbf{F}_{\mathrm{BB},m}}\frac{1}{K}\sum_{k=0}^{K-1}\mathcal{B}_m(\vartheta_k) - \mu_{\mathrm{SI}}\nabla_{\mathbf{F}_{\mathrm{BB},m}}\mathcal{S}_m\Bigg), \end{aligned} \tag{20}$$

where the expressions for the gradients $\nabla_{\mathbf{F}_{\mathrm{BB},m}}\mathcal{R}_{u,m}$, $\nabla_{\mathbf{F}_{\mathrm{BB},m}}\mathcal{B}_m(\vartheta_k)$ and $\nabla_{\mathbf{F}_{\mathrm{BB},m}}\mathcal{S}_m$ are expressed as

$$\begin{aligned} \nabla_{\mathbf{F}_{\mathrm{BB},m}}\mathcal{R}_{u,m} = &\frac{\mathbf{F}_{\mathrm{RF}}^{\mathrm{H}}\bar{\mathbf{h}}_{\mathrm{dl},u,m}\bar{\mathbf{h}}_{\mathrm{dl},u,m}^{\mathrm{H}}\mathbf{F}_{\mathrm{RF}}\mathbf{F}_{\mathrm{BB},m}}{\ln 2\cdot\left(\left\|\bar{\mathbf{h}}_{\mathrm{dl},u,m}^{\mathrm{H}}\mathbf{F}_{\mathrm{RF}}\mathbf{F}_{\mathrm{BB},m}\right\|^2 + \bar{\sigma}_u^2\right)} \\ &- \frac{\mathbf{F}_{\mathrm{RF}}^{\mathrm{H}}\bar{\mathbf{h}}_{\mathrm{dl},u,m}\bar{\mathbf{h}}_{\mathrm{dl},u,m}^{\mathrm{H}}\mathbf{F}_{\mathrm{RF}}\mathbf{F}_{\mathrm{BB},m}\mathbf{E}_u}{\ln 2\cdot\left(\left\|\bar{\mathbf{h}}_{\mathrm{dl},u,m}^{\mathrm{H}}\mathbf{F}_{\mathrm{RF}}\mathbf{F}_{\mathrm{BB},m}\mathbf{E}_u\right\|^2 + \bar{\sigma}_u^2\right)}, \end{aligned} \tag{21}$$

$$\nabla_{\mathbf{F}_{\mathrm{BB},m}}\mathcal{B}_m(\vartheta_k) = -2\sqrt{\mathcal{B}_m(\vartheta_k)}\mathbf{F}_{\mathrm{RF}}^{\mathrm{H}}\mathbf{A}_{\mathrm{T}}(\vartheta_k)\mathbf{F}_{\mathrm{RF}}\mathbf{F}_{\mathrm{BB},m}, \tag{22}$$

$$\nabla_{\mathbf{F}_{\mathrm{BB},m}}\mathcal{S}_m = \mathbf{F}_{\mathrm{RF}}^{\mathrm{H}}\mathbf{H}_{\mathrm{SI},m}\mathbf{H}_{\mathrm{SI},m}^{\mathrm{H}}\mathbf{F}_{\mathrm{RF}}\mathbf{F}_{\mathrm{BB},m}. \tag{23}$$

The overall PGA algorithm is given in Algorithm 1. In this algorithm, we update the analog and digital precoders with the given gradients in the same iteration as done in [14]. The step sizes to update the analog and digital precoders at t-th iteration are denoted by $\beta_{\mathrm{RF}}^{(t)}$ and $\beta_{\mathrm{BB},m}^{(t)}$, respectively, which

Algorithm 1 Hybrid precoder design with PGA

Input: $\bar{\mathbf{h}}_{\mathrm{dl},u,m}$, $\mathbf{H}_{\mathrm{SI},m}$, $\mathbf{a}_{\mathrm{T}}(\vartheta_k)$, P_{t}, $\bar{\sigma}_u^2$, μ_{b}, γ, N_{SI}, α

Initialize: $\mathbf{F}_{\mathrm{RF}}^{(0)}$, $\mathbf{F}_{\mathrm{BB},m}^{(0)}$, μ_{SI}, $t=0$

while not converged **do**
- Compute $\nabla_{\mathbf{F}_{\mathrm{RF}}}\mathcal{C}$ with $\mathbf{F}_{\mathrm{RF}}^{(t)}$ and $\mathbf{F}_{\mathrm{BB},m}^{(t)}$
- $\mathbf{F}_{\mathrm{RF}}^{(t+1)} \leftarrow \mathbf{F}_{\mathrm{RF}}^{(t+1)} + \beta_{\mathrm{RF}}^{(t)} \nabla_{\mathbf{F}_{\mathrm{RF}}^{(t)}}\mathcal{C}$
- Project to unit circle: $\mathbf{F}_{\mathrm{RF}}^{(t+1)} \leftarrow \mathbf{F}_{\mathrm{RF}}^{(t+1)} \oslash \left|\mathbf{F}_{\mathrm{RF}}^{(t+1)}\right|$
- Compute $\nabla_{\mathbf{F}_{\mathrm{BB},m}}\mathcal{C}$ with $\mathbf{F}_{\mathrm{RF}}^{(t+1)}$ and $\mathbf{F}_{\mathrm{BB},m}^{(t)}$
- $\mathbf{F}_{\mathrm{BB},m}^{(t+1)} \leftarrow \mathbf{F}_{\mathrm{BB},m}^{(t+1)} + \beta_{\mathrm{BB},m}^{(t)} \nabla_{\mathbf{F}_{\mathrm{BB},m}^{(t)}}\mathcal{C}, \quad \forall m$
- Power normalization: $\mathbf{F}_{\mathrm{BB},m}^{(t+1)} \leftarrow \frac{\sqrt{P_{\mathrm{t}}}\mathbf{F}_{\mathrm{BB},m}^{(t+1)}}{\left\|\mathbf{F}_{\mathrm{RF}}^{(t+1)}\mathbf{F}_{\mathrm{BB},m}^{(t+1)}\right\|_{\mathrm{F}}}$
- **if** $\mathrm{mod}(t+1, N_{\mathrm{SI}}) = 0$ **and** $\max\left(\mathcal{S}_{p,m}^{(t+1)}\right) > \gamma$ **then**
  - $\mu_{\mathrm{SI}} \leftarrow \alpha\mu_{\mathrm{SI}}$
- **end if**
- Update the iteration index: $t \leftarrow t+1$

end while

Output: $\mathbf{F}_{\mathrm{RF}} = \mathbf{F}_{\mathrm{RF}}^{(t)}$, $\mathbf{F}_{\mathrm{BB},m} = \mathbf{F}_{\mathrm{BB},m}^{(t)}$

are updated via line search [15]. Moreover, we utilize an adaptive penalty weight for SI. The SI value is evaluated every N_{SI} iterations, and if the maximum SI at RX antennas is above the threshold γ, we multiply the SI penalty weight with $\alpha > 1$. Otherwise, the SI penalty weight remains constant.

B. Combiner Optimization

The combiner problem introduced in (14) ideally aims to maximize the sum UL spectral efficiency. However, the interference terms in the spectral efficiency expression in (11) include the sensing channel $\mathbf{A}_{m,n}$ in addition to the SI channel, while it is likely that this channel is not available since the goal is to estimate it. Therefore, we neglect the sensing channel in this expression, and denote the spectral efficiency expression without the sensing channel by $\tilde{\mathcal{R}}'_{\tilde{u},m}$, and the sum spectral efficiency by $\tilde{\mathcal{R}}'_m$. However, maximizing spectral efficiency without accounting for the sensing channel may degrade performance, particularly when targets are near the BS or UL UEs. To mitigate this, one approach is successive interference cancellation after sensing channel estimation. However, since our focus is on precoder and combiner design, we address this through digital combiner. Specifically, while analog combiners should have high gains at target directions, UL digital combiners should suppress them. This can be achieved via a zero-forcing (ZF) constraint such that $\mathbf{W}_{\mathrm{BB},m}^{\mathrm{H}}\mathbf{W}_{\mathrm{RF}}^{\mathrm{H}}\tilde{\mathbf{A}} = \mathbf{0}$, where $\tilde{\mathbf{A}} = [\mathbf{a}_{\mathrm{R}}(\vartheta_0), \ldots, \mathbf{a}_{\mathrm{R}}(\vartheta_{K-1})]$. We employ a null-space projection method [3], defining the digital combiners as $\mathbf{w}_{\mathrm{BB},\tilde{u},m} = \mathbf{N}^{\mathrm{H}}\tilde{\mathbf{w}}_{\mathrm{BB},\tilde{u},m}$, with $\mathbf{N} = \mathbf{I} - \mathbf{W}_{\mathrm{RF}}^{\mathrm{H}}\tilde{\mathbf{A}}(\mathbf{W}_{\mathrm{RF}}^{\mathrm{H}}\tilde{\mathbf{A}})^{\dagger}$ and auxiliary variable $\tilde{\mathbf{w}}_{\mathrm{BB},\tilde{u},m} \in \mathbb{C}^{N_{\mathrm{RF}}}$. Thus, we optimize $\tilde{\mathbf{w}}_{\mathrm{BB},\tilde{u},m}$ in the null-space of target angles and recover $\mathbf{w}_{\mathrm{BB},\tilde{u},m}$ accordingly. Additionally, we move the residual SI constraint to the objective function by utilizing a common penalty weight $\tilde{\mu}_{\mathrm{SI}}$ for all RF chains. This is given by

$$\begin{aligned} \underset{\mathbf{W}_{\mathrm{RF}},\tilde{\mathbf{w}}_{\mathrm{BB},\tilde{u},m}}{\text{maximize}} \quad & \frac{1}{M}\sum_{m=0}^{M-1}\left(\tilde{\mathcal{R}}'_m - \tilde{\mu}_{\mathrm{SI}}\tilde{\mathcal{S}}_m\right) - \tilde{\mu}_{\mathrm{b}}\tilde{\mathcal{B}}(\vartheta_k) \\ \text{subject to} \quad & |[\mathbf{W}_{\mathrm{RF}}]_{p,q}| = 1, \ \forall p,q, \end{aligned} \tag{24}$$

where $\tilde{\mathcal{S}}_m = \sum_{q=1}^{N_{\mathrm{RF}}}\tilde{\mathcal{S}}_{q,m} = \left\|\mathbf{W}_{\mathrm{RF}}^{\mathrm{H}}\mathbf{H}_{\mathrm{SI},m}\mathbf{F}_{\mathrm{RF}}\mathbf{F}_{\mathrm{BB},m}\right\|_{\mathrm{F}}^2$. The same PGA algorithm can be used to design the hybrid combiners. Note that the digital combiners do not have a power constraint unlike the digital precoders. In addition, digital combiners are only involved in the spectral efficiency expression, and their optimization are independent for different UL UEs. Thus, we can find the closed-form solution to the auxiliary digital combiners as

$$\tilde{\mathbf{w}}_{\mathrm{BB},\tilde{u},m} = \left(\tilde{\mathbf{W}}_{\mathrm{RF}}^{\mathrm{H}}\mathbf{R}_{\tilde{u},m}\tilde{\mathbf{W}}_{\mathrm{RF}}\right)^{-1}\tilde{\mathbf{W}}_{\mathrm{RF}}^{\mathrm{H}}\bar{\mathbf{h}}_{\mathrm{ul},\tilde{u},m}, \tag{25}$$

where $\tilde{\mathbf{W}}_{\mathrm{RF}} = \mathbf{W}_{\mathrm{RF}}\mathbf{N}^{\mathrm{H}}$. Additionally, the interference covariance can be expressed as

$$\begin{aligned} \mathbf{R}_{\tilde{u},m} = {} & \bar{\mathbf{H}}_{\mathrm{ul},m}\mathbf{E}_{\tilde{u}}\bar{\mathbf{H}}_{\mathrm{ul},m}^{\mathrm{H}} \\ & + \mathbf{H}_{\mathrm{SI},m}\mathbf{F}_{\mathrm{RF}}\mathbf{F}_{\mathrm{BB},m}\mathbf{F}_{\mathrm{BB},m}^{\mathrm{H}}\mathbf{F}_{\mathrm{RF}}^{\mathrm{H}}\mathbf{H}_{\mathrm{SI},m}^{\mathrm{H}} + \tilde{\sigma}^2\mathbf{I}, \end{aligned} \tag{26}$$

where the overall effective UL channel is defined as $\bar{\mathbf{H}}_{\mathrm{ul},m} = \left[\bar{\mathbf{h}}_{\mathrm{ul},1,m}, \cdots, \bar{\mathbf{h}}_{\mathrm{ul},\tilde{U},m}\right]$. We propose to utilize a variation of Algorithm 1 such that the analog combiner is optimized via PGA while the digital combiners are updated by using the closed-form solution in (25). The rest of the algorithm follows the same steps. For example, we utilize an adaptive SI weight $\tilde{\mu}_{\mathrm{SI}}$ so that the maximum SI observed at RF chains is below $\tilde{\gamma}$. While the gradient expression for the analog combiner is omitted for brevity, it can be obtained similar to (16).

V. Numerical Results

In this section, we investigate the performance of the proposed design. The carrier frequency is set to 28 GHz, while the number of OFDM symbols and the number of subcarriers are selected as $N=14$ and $M=128$, respectively, with subcarrier spacing $\Delta f = 480$ kHz and symbol duration $T_{\mathrm{s}} = 2.67\,\mu$s. The FD BS is equipped with two ULAs that are separated by 2λ. The number of antennas and the number of RF chains at the BS are $N_{\mathrm{T}} = N_{\mathrm{R}} = 64$ and $N_{\mathrm{RF}} = 8$ RF, respectively. In addition, there are 2 DL and 2 UL UEs that are equipped with $N_{\mathrm{u}} = 2$ antennas. We consider $K=3$ point targets with radar cross-section of $10\,\mathrm{m}^2$. The target angles and LoS angles of UEs are randomly selected from $[-60^\circ, 60^\circ]$. Moreover, the range of the targets and UE locations, and the velocity of the targets are randomly selected from $[40\,\mathrm{m}, 60\,\mathrm{m}]$ and $[10\,\mathrm{m/s}, 30\,\mathrm{m/s}]$, respectively. The angles of the four NLoS paths are randomly selected from $[-90^\circ, 90^\circ]$, while their gains are 5-15dB below the gain of the LoS path. The transmit power at the BS and UL UEs are set to $P_{\mathrm{t}} = 23$ dBm and $\tilde{P}_{\mathrm{t},\tilde{u}} = 10$ dBm, respectively. The optimization parameters are selected as follows: $\mu_{\mathrm{b}} = 0.1/P_{\mathrm{t}}$, $\mu_{\mathrm{SI}} = 10^5$, $\tilde{\mu}_{\mathrm{b}} = 1/(N_{\mathrm{R}}N_{\mathrm{RF}})^2$, $\tilde{\mu}_{\mathrm{SI}} = 10^6$, $N_{\mathrm{SI}} = 10$, $\alpha = 10$, $\gamma = 10^6\bar{\sigma}^2$, and $\tilde{\gamma} = 10^4 N_{\mathrm{R}}\tilde{\sigma}^2$. The precoders and combiners are initialized via the hybrid factorization of the fully digital ZF solution [17].

Fig. 1 shows the performance of the proposed architecture with various metrics. First, we investigate the convergence

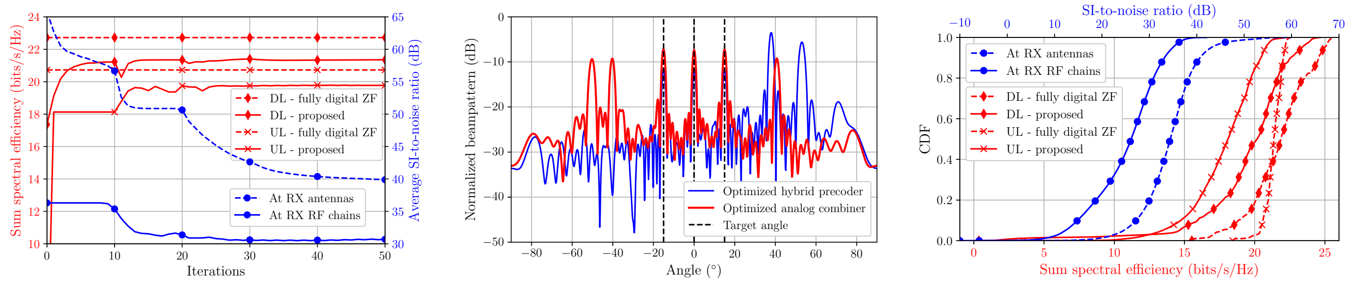

(a) (b) (c)

Fig. 1. Performance evaluation of the proposed algorithm: (a) sample sum spectral efficiency and average SI-to-noise ratio vs iterations, (b) sample normalized TX and RX beampatterns, and (c) CDF of the sum spectral efficiency and SI-to-noise ratio obtained with 100 channel realizations.

behavior of the proposed algorithm in Fig. 1a. It can be observed that both the DL and UL sum spectral efficiency converges after 20 iterations, while their gap to the half-duplex fully digital ZF benchmark is reasonable small. Similar convergence behavior is observed for the average SI-to-noise ratio at RX antennas and at RX RF chains. Furthermore, normalized beampatterns of the hybrid precoder and analog combiner are given in Fig. 1b. We observe that there are significant peaks at target angles, and there are additional peaks for communication paths. Finally, the CDF of the DL/UL sum spectral efficiency and SI-to-noise ratio are given in Fig. 1c. While there is a reasonable degradation in spectral efficiency, this gap can be tuned via μ_b and $\tilde{\mu}_\mathrm{b}$ which adjust the trade-off between sensing and communication. If these values are increased, the spectral efficiency would decrease while magnitudes of the beampattern peaks observed at target angles would increase. Moreover, the SI-to-noise ratio at RX antennas and RX RF chains are below 60 dB and 40 dB, as enforced by the thresholds γ and $\tilde{\gamma}$, respectively. This result shows that the proposed optimization framework is able to effectively suppress the SI before LNAs and ADCs.

VI. Conclusion

In this paper, we proposed a hybrid precoding and combining design for FD ISAC systems to effectively suppress the SI at RX antennas (i.e., before LNAs), and after analog combining (i.e., before ADCs). Using a penalty-based PGA algorithm, the proposed algorithm achieves a balance between communication and sensing. Simulation results confirm rapid convergence and performance near that of fully digital solutions, demonstrating the practical viability of the proposed hybrid architecture for next-generation FD ISAC systems. Future research directions include accounting for imperfect channel estimation, and analyzing and reducing the computational complexity per iteration to lower overall runtime and improve scalability.

References

[1] N. González-Prelcic *et al.*, "The integrated sensing and communication revolution for 6G: Vision, techniques, and applications," *Proc. IEEE*, vol. 112, no. 7, pp. 676–723, 2024.

[2] C. B. Barneto, S. D. Liyanaarachchi, M. Heino, T. Riihonen, and M. Valkama, "Full duplex radio/radar technology: The enabler for advanced joint communication and sensing," *IEEE Wireless Commun.*, vol. 28, no. 1, pp. 82–88, 2021.

[3] C. B. Barneto, T. Riihonen, S. D. Liyanaarachchi, M. Heino, N. González-Prelcic, and M. Valkama, "Beamformer design and optimization for joint communication and full-duplex sensing at mm-Waves," *IEEE Trans. Commun.*, vol. 70, no. 12, pp. 8298–8312, 2022.

[4] M. A. Islam, G. C. Alexandropoulos, and B. Smida, "Integrated sensing and communication with millimeter wave full duplex hybrid beamforming," in *Proc. IEEE Int. Conf. Commun. (ICC)*, 2022, pp. 4673–4678.

[5] M. Bayraktar, N. González-Prelcic, and H. Chen, "Hybrid precoding and combining for mmWave full-duplex joint radar and communication systems under self-interference," in *Proc. IEEE Int. Conf. Commun. (ICC)*, 2024, pp. 915–920.

[6] Z. Liu, S. Aditya, H. Li, and B. Clerckx, "Joint transmit and receive beamforming design in full-duplex integrated sensing and communications," *IEEE J. Sel. Areas Commun.*, vol. 41, no. 9, pp. 2907–2919, 2023.

[7] Z. He, W. Xu, H. Shen, D. W. K. Ng, Y. C. Eldar, and X. You, "Full-duplex communication for ISAC: Joint beamforming and power optimization," *IEEE J. Sel. Areas Commun.*, vol. 41, no. 9, pp. 2920–2936, 2023.

[8] M. T. Kabir, A. Gaydamaka, D. Moltchanov, M. Valkama, and B. Tan, "Beamforming and Tx power optimization for FD-ISAC with inter- and co-channel interference," *Electron. Lett.*, vol. 61, no. 1, p. e70138, 2025.

[9] M. Bayraktar, N. González-Prelcic, H. Chen, and C. J. Zhang, "Truly full-duplex integrated sensing and single-user communication at mmWave," in *Proc. IEEE 25th Int. Workshop Signal Process. Advances Wireless Commun. (SPAWC)*, 2024, pp. 116–120.

[10] K. Park, J. Myeong, G. M. Rebeiz, and B.-W. Min, "A 28-GHz full-duplex phased array front-end using two cross-polarized arrays and a canceller," *IEEE Trans. Microw. Theory Techn.*, vol. 69, no. 1, pp. 1127–1135, 2021.

[11] M. Cui, L. Dai, Z. Wang, S. Zhou, and N. Ge, "Near-field rainbow: Wideband beam training for XL-MIMO," *IEEE Trans. Wireless Commun.*, vol. 22, no. 6, pp. 3899–3912, 2023.

[12] F. Liu, L. Zhou, C. Masouros, A. Li, W. Luo, and A. Petropulu, "Toward dual-functional radar-communication systems: Optimal waveform design," *IEEE Trans. Signal Process.*, vol. 66, no. 16, pp. 4264–4279, 2018.

[13] J. A. Zhang, X. Huang, Y. J. Guo, J. Yuan, and R. W. Heath, "Multibeam for joint communication and radar sensing using steerable analog antenna arrays," *IEEE Trans. Veh. Technol.*, vol. 68, no. 1, pp. 671–685, 2019.

[14] N. T. Nguyen, L. V. Nguyen, N. Shlezinger, Y. C. Eldar, A. L. Swindlehurst, and M. Juntti, "Joint communications and sensing hybrid beamforming design via deep unfolding," *IEEE J. Sel. Topics Signal Process.*, 2024.

[15] D. P. Bertsekas, *Nonlinear Programming*, 2nd ed. Belmont, MA: Athena Scientific, 1999.

[16] J. Nocedal and S. J. Wright, *Numerical optimization*. Springer Science, 2006.

[17] J. Rodriguez-Fernández and N. González-Prelcic, "Low-complexity multiuser hybrid precoding and combining for frequency selective millimeter wave systems," in *Proc. IEEE 19th Int. Workshop Signal Process. Advances Wireless Commun. (SPAWC)*, 2018, pp. 1–5.